Simulation of structural and electronic properties of amorphous tungsten oxycarbides

2012 New J. Phys. 14 113028

(http://iopscience.iop.org/1367-2630/14/11/113028)

New Journal of Physics
The open access journal for physics

Simulation of structural and electronic properties of amorphous tungsten oxycarbides

Kaliappan Muthukumar, Roser Valentí and Harald O Jeschke[1]
Institut für Theoretische Physik, Goethe-Universität Frankfurt am Main,
D-60438 Frankfurt am Main, Germany
E-mail: jeschke@itp.uni-frankfurt.de

New Journal of Physics **14** (2012) 113028 (13pp)
Received 30 July 2012
Published 22 November 2012
Online at http://www.njp.org/
doi:10.1088/1367-2630/14/11/113028

Abstract. Electron beam-induced deposition with tungsten hexacarbonyl $W(CO)_6$ as precursors leads to granular deposits with varying compositions of tungsten, carbon and oxygen. Depending on the deposition conditions, the deposits are insulating or metallic. We employ an evolutionary algorithm to predict the crystal structures starting from a series of chemical compositions that were determined experimentally. We show that this method leads to better structures than structural relaxation based on estimated initial structures. We approximate the expected amorphous structures by reasonably large unit cells that can accommodate local structural environments that resemble the true amorphous structure. Our predicted structures show an insulator-to-metal transition close to the experimental composition at which this transition is actually observed and they also allow comparison with experimental electron diffraction patterns.

[1] Author to whom any correspondence should be addressed.

Contents

1. Introduction

Nanotechnological applications require the fabrication of nanometer-sized structures on various substrates. Electron beam-induced deposition (EBID) has emerged as a promising technique to make nanostructures in a size, shape and position-controlled manner without the use of expensive masks [1–5]. Deposits with the desired metal content and electronic properties can be obtained either directly by tuning the preparation conditions (varying the electron beam energy) or by post-fabrication techniques (heating or further irradiation). Thus, fabrication of materials with new physical and chemical properties at the nanoscale has been successfully achieved [3, 5–10].

Transition metal carbides possess unique physical and chemical properties that have made them promising materials in several industrial and electronic applications. The composition of tungsten granular deposits obtained by decomposing $W(CO)_6$ as a precursor in the EBID process indicates that the tungsten atoms are embedded in a carbon (and oxygen) matrix [3]. Although investigations on the microstructure and the electrical transport properties have shed some light on the behavior of these systems, a deep microscopic understanding is still missing.

Several theoretical studies are available on the structural and electronic properties of 4d and 5d transition metal carbides [11, 12]. Nevertheless, studies on metal oxycarbides are scarce due to the lack of knowledge about their structures. The high level of carbon and oxygen concentrations up to an average of 30–40% in the EBID-fabricated samples indicates that a good description of the electronic structure of these metal oxycarbides may be obtained by suitably estimating approximate structures from the well-known crystal structures of tungsten carbides and tungsten oxides. This methodology has indeed been successful in predicting the structure of Pt_2Si_3 derived from Pt_2Sn_3 [13]. A similar procedure for tungsten oxycarbides has been adapted by Suetin *et al*, who investigated the structure, electronic and magnetic properties of some tungsten oxycarbides by constructing approximate crystal structures obtained from systematically replacing the carbon by oxygen in the hexagonal structure of WC and oxygen by carbon in the cubic structure WO_3 [14]. However, a powerful evolutionary algorithm was recently proposed, which, in principle, can predict the crystal structure of materials with any atomic composition and is not biased by the choice of the initially known crystal structure settings [15–17].

In this work, we use this evolutionary algorithm to predict structures of approximants representing amorphous tungsten oxycarbides as obtained by the EBID process using periodic boundary conditions (i.e. we simulate an amorphous compound with a crystalline system). By analyzing the electronic properties of our predicted structures, we find an insulator-to-metal transition at a composition close to the composition where experimentally such a transition

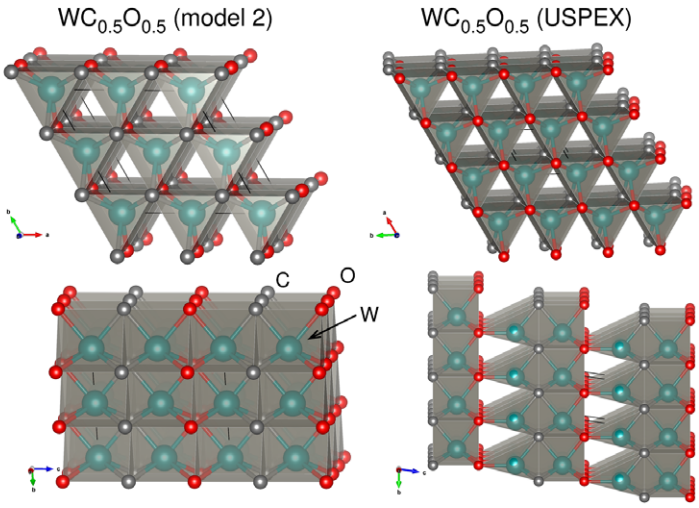

Figure 1. Predicted structures for the tungsten oxycarbide $WC_{0.5}O_{0.5}$. Left: the best structure obtained by relaxing estimated candidate structures. Right: USPEX result. Colors used throughout this work are gray for carbon, red for oxygen and turquoise for tungsten.

Table 1. EBID-obtained samples as reported in [6] and the corresponding approximant used for the structure prediction. The concentrations are given in atomic %. The composition of the approximants normalized to the tungsten content is also listed.

Sample	W	C	O	Approximant	Approximant composition
1	19.0	67.1	13.8	$W_3C_{10}O_2$	$WC_{3.33}O_{0.67}$
2	22.6	56.0	21.4	$W_2C_5O_2$	$WC_{2.5}O$
3	27.5	50.4	22.1	$W_4C_7O_3$	$WC_{1.75}O_{0.75}$
4	31.8	44.4	23.8	$W_5C_7O_4$	$WC_{1.4}O_{0.8}$
5	34.0	44.3	21.7	$W_3C_4O_2$	$WC_{1.33}O_{0.67}$
6	36.9	35.6	27.5	$W_7C_7O_5$	$WCO_{0.71}$

has been observed [6]. We further show that the calculated electron diffraction patterns for our structures correlate very well with the patterns measured experimentally [3, 6].

2. Method

We approximated the amorphous tungsten oxycarbides structures obtained in the EBID process by large unit cells that can account for the local structural environment present in the experimental compositions. In order to predict these structures, we employed the Universal Structure Predictor: Evolutionary Xtallography package (USPEX) developed by Oganov *et al*. This code is based on evolutionary algorithms and features local optimization, real-space representation and flexible physically motivated variation operators [15–17]. Each generation contained between 20 and 40 structures and the first generation was always

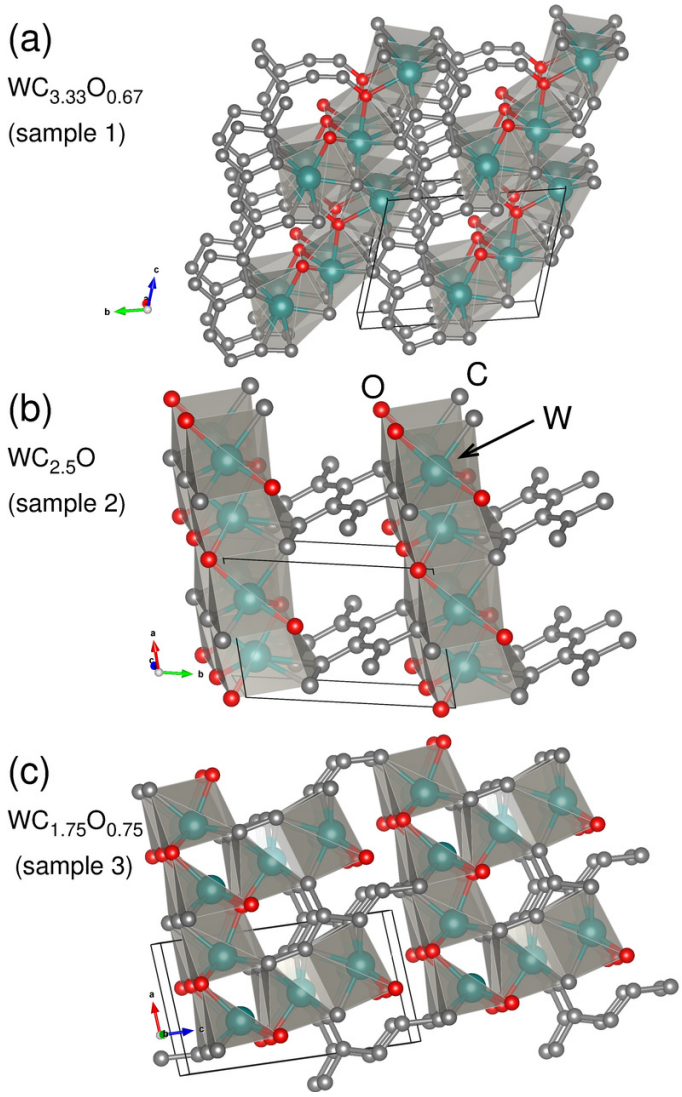

Figure 2. Predicted tungsten oxycarbide structures for the compositions $WC_{3.33}O_{0.67}$, $WC_{2.5}O$ and $WC_{1.75}O_{0.75}$.

produced randomly. Three different sets of calculation have been performed for each composition with a differing number of initial populations and slightly varying the parameter (fracPerm) that controls the percentage of structures obtained by heredity and permutation. With all these different sets of calculation, about 2000 structures were screened for each composition. All structures were locally optimized during structure search using density functional theory with the projector augmented wave [18, 19] as implemented in the Vienna *ab initio* simulation package (VASP) [19–22]. The generalized gradient approximation (GGA) in the parametrization of Perdew *et al* [23] was used as an approximation for the exchange and correlation functional. The reported structures are the ones with the lowest enthalpy; the evolutionary algorithm was considered converged when the lowest enthalpy

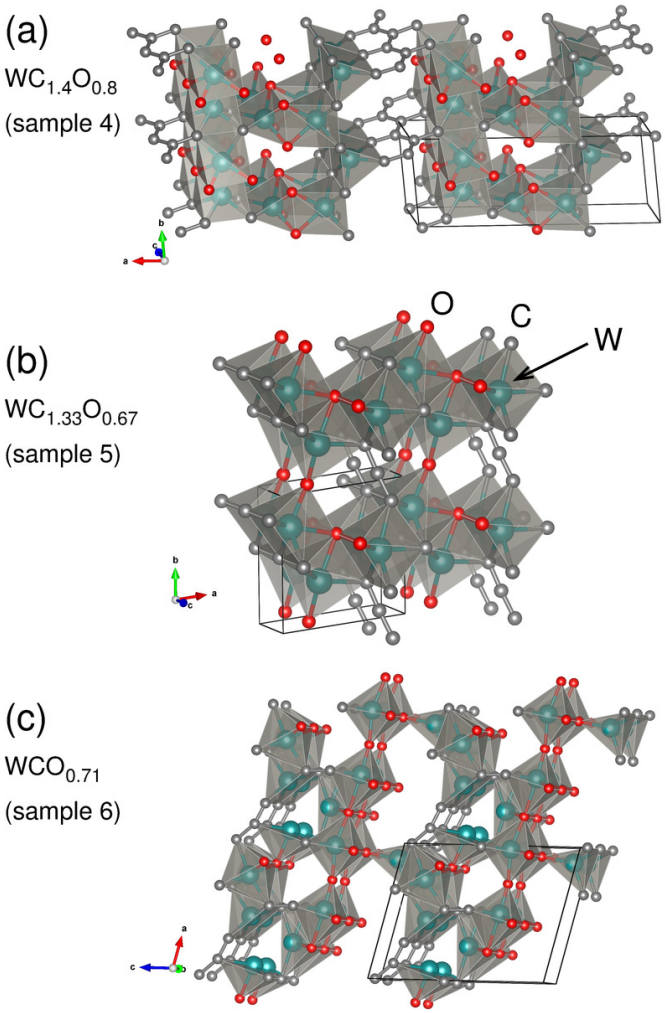

Figure 3. Predicted tungsten oxycarbide structures for the compositions $WC_{1.4}O_{0.8}$, $WC_{1.33}O_{0.67}$ and $WCO_{0.71}$.

structure could not be improved during eight generations[2]. We analyzed the electronic structure of the resulting structures using the full potential local orbital (FPLO) basis [24]. The electron diffraction patterns were simulated by the Reflex module implemented in the Materials Studio package.

3. Results and discussion

We first tested the method of evolutionary algorithm-based structure prediction using some known tungsten structures. As an example, we verified that USPEX indeed predicts the known hexagonal structure of WC [26]. Next, we address the problem of predicting crystalline tungsten oxycarbides. This has recently been discussed by Suetin *et al* [14] for the examples $WC_{1-x}O_x$ and $WC_{3-x}O_x$. The authors successively replace carbon atoms in WC with oxygen and replace

[2] We would like to note that by further improving the converge criteria of the generic algorithm, one could, in principle, find even more stable structures. But we found that the used generic algorithm reproduces reasonably well the experimental observations as shown below and is still computationally feasible.

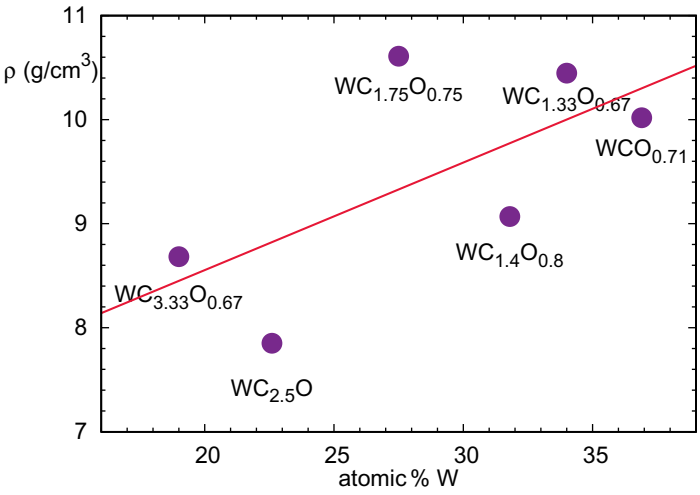

Figure 4. The density of the predicted tungsten oxycarbide structures roughly increases with tungsten content.

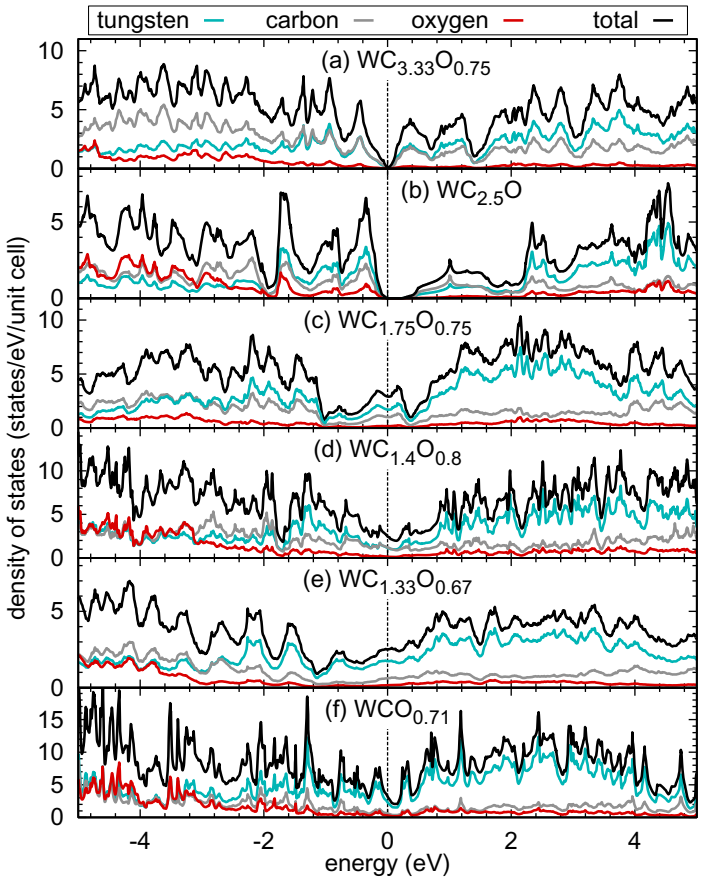

Figure 5. Electronic density of states of the predicted tungsten oxycarbide structures.

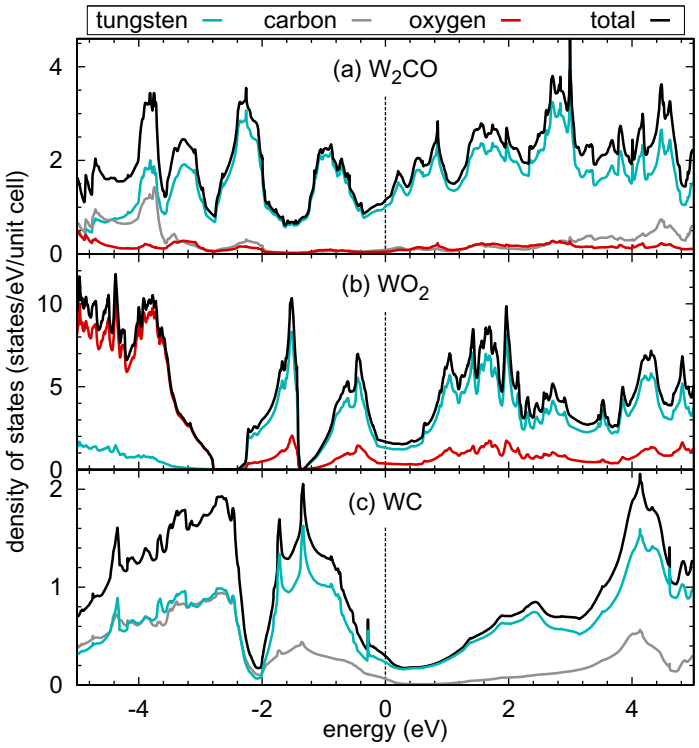

Figure 6. Electronic density of states of (a) the predicted structure of W_2CO and of the known crystalline structures of WO_2 (b) and WC (c).

oxygen atoms in WO_3 by carbon atoms and relax the resulting structure candidates using the full potential linearized augmented plane wave basis set. We verified that the structure of $WC_{0.5}O_{0.5}$ with alternating layers of WC and WO (figure 1 (left)) is indeed the optimal structure also when relaxing different structure candidates using VASP. We then performed an USPEX structure prediction with the composition W_2CO. This yields as optimum the structure shown in figure 1 (right). It is triclinic ($P1$ symmetry) and it is 1.35 eV per W_2CO unit lower in energy than the high-symmetry ($P\text{-}6m2$) structure obtained by relaxing structure candidates (figure 1 (left)). This indicates that indeed it is preferable to avoid bias by using a structure search based on evolutionary principles.

Figures 2 and 3 show the structures that we obtained. The samples with high carbon content show inclusions of regions that resemble diamond-like carbon (sample 1) or graphitic carbon (samples 2 and 4). This leads to a lower density as can be seen from figure 4 in which the density of amorphous tungsten oxycarbide approximants is plotted against the metal content. On the one hand, there is a weak overall proportionality of density with tungsten content, illustrated by the line fitted to the six data points. On the other hand, samples 1, 2 and 4 fall into a lower density group ($WC_{3.33}O_{0.67}$, $WC_{2.5}O$ and $WC_{1.4}O_{0.8}$, ρ ranges from 7.8 to 9.1 g cm^{-3}), which shows some phase separation between low carbon content tungsten oxycarbide and regions of pure carbon, and a higher density group, samples 3, 5 and 6 ($WC_{1.75}O_{0.75}$, $WC_{1.33}O_{0.67}$ and $WCO_{0.71}$, ρ ranges from 10.0 to 10.7 g cm^{-3}), which is more homogeneous and more highly coordinated. By inspecting second best solutions which the evolutionary algorithm always provides, we find that the overall trend of figure 4 is confirmed but densities carry an error of approximately ± 0.5 g cm^{-3}. Simulation of larger unit cells would be required to reduce this error.

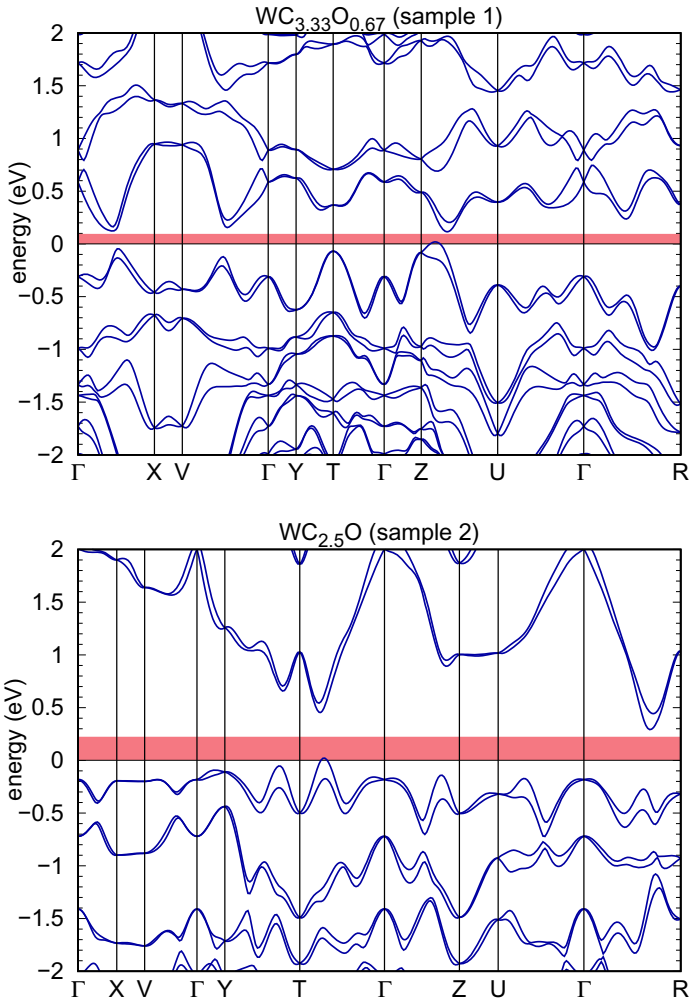

Figure 7. Band structures of the two insulating compounds $WC_{3.33}O_{0.67}$ (top) and $WC_{2.5}O$.

We now investigate the electronic structure of the predicted amorphous tungsten oxycarbide approximants. We employ the FPLO basis [24] within GGA. Due to the large mass of tungsten, we compared scalar relativistic and fully relativistic electronic structure calculations. We find significant splittings due to spin–orbit coupling in all band structures, and therefore in the following we base our analysis on fully relativistic calculations. Figure 5 shows a comparison of the densities of states of the six materials with tungsten, carbon and oxygen contributions shown in different colors. We immediately observe an insulator-to-metal transition between sample 2 ($WC_{2.5}O$) and sample 3 ($WC_{1.75}O_{0.75}$) which corresponds to a transition between 22 and 29% metal content. This is in excellent agreement with the observation by Huth *et al* [6] where the conductivity measurements on the six samples (see table 1) showed a change from insulating to metallic behavior between samples 3 and 4. In fact, figure 2 of [6] shows that sample 3 takes an intermediate position between clearly finite conductivity in the $T \to 0$ limit for sample 4 and clearly vanishing conductivity in the $T \to 0$ limit for sample 2.

For comparison we present in figure 6 the densities of states for the predicted crystalline structure of our test system W_2CO as well as for the known structures of WO_2 [25] and WC [26]. We observe a qualitatively different behavior for the three structures.

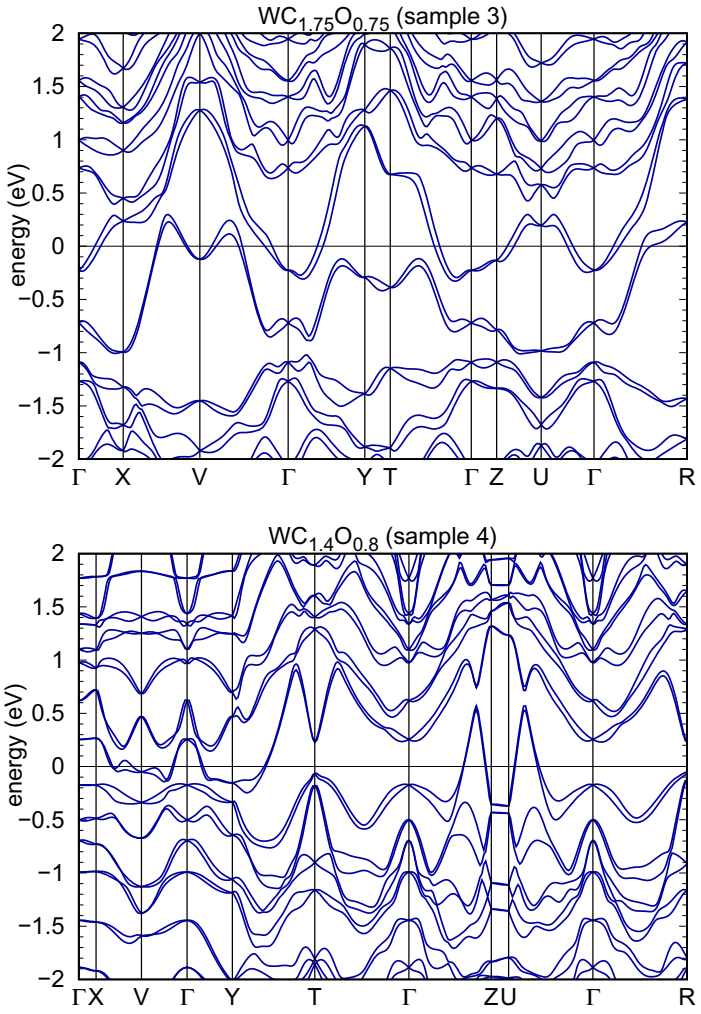

Figure 8. Band structures of the two metallic compounds $WC_{1.75}O_{0.75}$ (top) and $WC_{1.4}O_{0.8}$. Compounds with higher relative tungsten content are also metallic.

In figures 7 and 8, we show the calculated band structures for the first four predicted structures. Here, we can also clearly see the transition from insulating to metallic behavior upon an increase of tungsten content as well as the splitting of the bands due to the spin–orbit coupling. We also observe highly dispersive bands, which are a signature of the three dimensionality of the systems.

In order to check how good our simulated structures describe the amorphous deposits, we present in figures 9 and 10 the pair correlation functions of the first four predicted structures. The pair correlation functions are used here to characterize the local environment around the metal atoms. Experimentally, it is of course very difficult to measure pair correlation functions for nanometer-sized deposits. However, our purpose here is to exploit the additional knowledge we have from our microscopic simulations and to provide an estimate of the nature of the bonds (i.e., W–C or W–O or W–W); this is a comment on the related discussion in the experimental work of [27]. In figures 9 and 10, the contributions of bonds involving tungsten are highlighted. The pair correlation function first shows carbon–carbon bonds at 1.4–1.5 Å, indicating that the

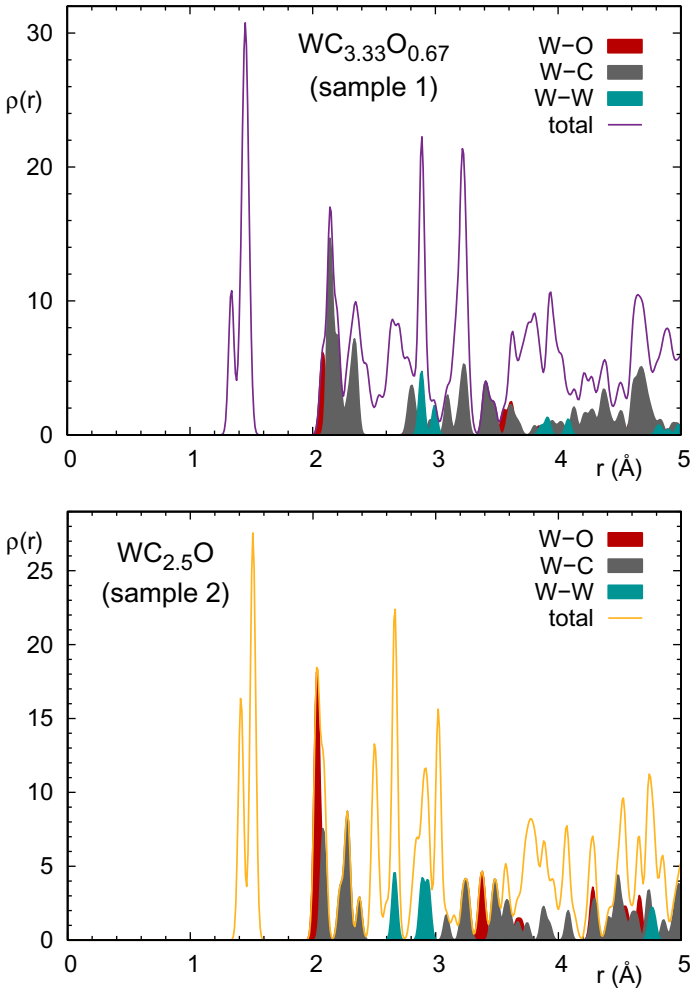

Figure 9. Pair correlation functions of the compounds $WC_{3.33}O_{0.67}$ (top) and $WC_{2.5}O$.

matrix is composed of carbon atoms with sp^2 and sp^3 hybridization, which is in accordance with the experimental evidence based on micro-Raman measurements on tungsten-based composites obtained in the EBID process [27]. Further analysis indicates that at 2.0 Å, there are W–O bonds, followed by W–C bonds at slightly larger distances. The first W–W bonds are seen at 2.6 Å.

Finally, we can compare our predicted structures with experiment by calculating the electron diffraction patterns. Figure 11 shows the predicted electron diffraction patterns for electrons with an energy of 300 keV. The experimental data shown in the figure are from [27]. Note that the experimental diffraction pattern has a large background that was not subtracted. We find very good agreement between the main peak observed experimentally at 4 nm^{-1} and the peaks in the predicted diffraction patterns. This peak corresponds to bond lengths of 2.5 Å and should be related to tungsten bonds as the light elements contribute only insignificantly to the electron diffraction intensity at 300 keV. Thus, we can relate the electron diffraction pattern to the pair correlation functions of figures 9 and 10 and conclude that the W–W bonds most likely cause the electron diffraction peak observed experimentally.

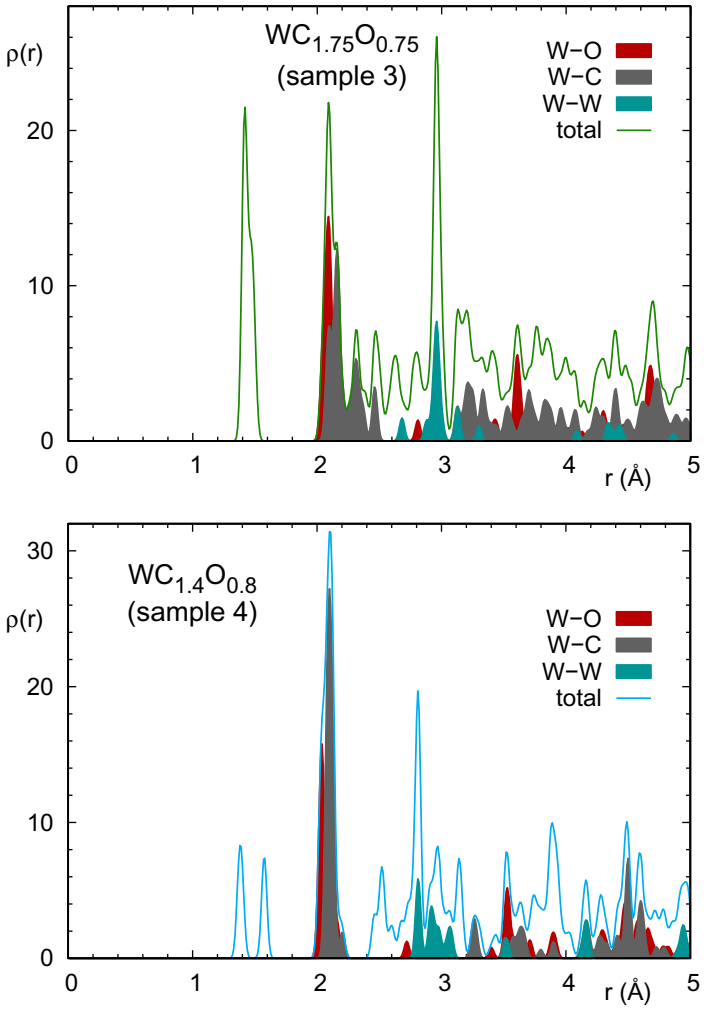

Figure 10. Pair correlation functions of the compounds $WC_{1.75}O_{0.75}$ (top) and $WC_{1.4}O_{0.8}$.

4. Conclusions

By employing evolutionary algorithms we have predicted structures of approximants to EBID-based amorphous tungsten oxycarbides. By analyzing the electronic structure, pair correlation functions and diffraction patterns of our predicted structures for different compositions of W, C and O, we find very good agreement with the experimental observations; an insulator-to-metal transition is observed at a concentration close to the experimental concentration at which this transition is reported and we explain the prominent peak observed in transmission electron microscope based electron diffraction as caused by W–W bonds.

The use of genetic algorithms to predict and simulate amorphous nanodeposits opens the possibility to understand the microscopic origin of the behavior of these systems. This has been, up to now, very limited and mostly restricted to phenomenological models. With this tool at hand, we believe that important progress can be made in this field.

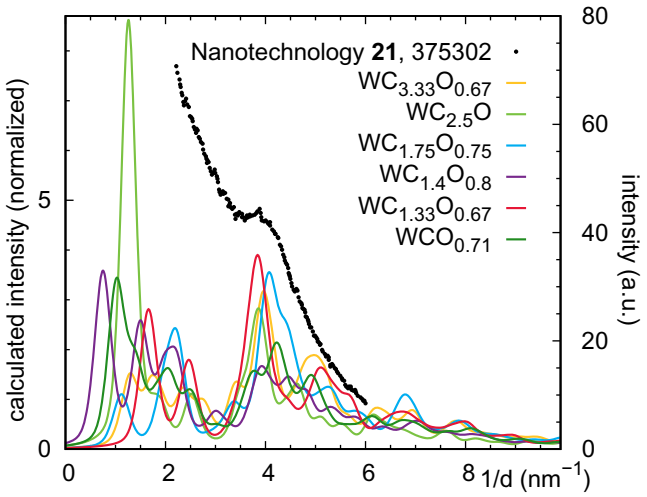

Figure 11. Calculated electron diffraction intensities (lines) for an electron energy of $E = 300\,\mathrm{keV}$, compared to the measured diffraction pattern of [27].

Acknowledgments

The authors thank A Oganov for kindly supplying the code and Q Zhu, A Lyakhov and M Huth for useful discussions. We gratefully acknowledge financial support from the Beilstein-Institut, Frankfurt/Main, Germany, within the research collaboration NanoBiC. This work was supported by the Alliance Program of the Helmholtz Association (HA216/EMMI). Allotment of computer time by CSC-Frankfurt and LOEWE-CSC is gratefully acknowledged. Structure figures were prepared with VESTA 3 [28].

References

[1] Randolph S J, Fowlkes J D and Rack P D 2006 Focused, nanoscale electron-beam-induced deposition and etching *Crit. Rev. Solid State Mater. Sci.* **31** 55

[2] Silvis-Cividjian N, Hagen C W and Kruit P 2005 Spatial resolution limits in electron-beam-induced deposition *J. Appl. Phys.* **98** 084905

[3] Porrati F, Sachser R and Huth M 2009 The transient electrical conductivity of W-based electron-beam-induced deposits during growth, irradiation and exposure to air *Nanotechnology* **20** 195301

[4] Wnuk J D, Rosenberg S G, Gorham J M, van Dorp W F, Hagen C W and Fairbrother D H 2011 Electron beam deposition for nanofabrication: insights from surface science *Surf. Sci.* **605** 257

[5] Utke I, Hoffmann P and Melngailis J 2008 Gas-assisted focused electron beam and ion beam processing and fabrication *J. Vac. Sci. Technol.* B **26** 1197

[6] Huth M, Klingenberger D, Grimm C, Porrati F and Sachser R 2009 Conductance regimes of W-based granular metals prepared by electron beam induced deposition *New J. Phys.* **11** 033032

[7] van Dorp W F, van Someren B, Hagen C W, Kruit P and Crozier A P 2005 Approaching the resolution limit of nanometer-scale electron beam-induced deposition *Nano Lett.* **7** 1303

[8] van Dorp W F and Hagen C W 2008 A critical literature review of focused electron beam induced deposition *J. Appl. Phys.* **104** 081301

[9] Porrati F, Sachser R, Schwalb C H, Frangakis A S and Huth M 2011 Tuning the electrical conductivity of Pt-containing granular metals by postgrowth electron irradiation *J. Appl. Phys.* **109** 063715

[10] Donev E U and Hastings J T 2009 Electron-beam-induced deposition of platinum from a liquid precursor *Nano Lett.* **9** 2715
[11] Shaposhnikov V L, Migas D B, Rodin V N and Borisenko V E 2011 *Ab initio* investigation of structural and electronic properties of tungsten dioxide *Phys. Status Solidi* b **248** 1471
[12] Suetin D V, Shein I R and Ivanovskii A L 2010 Tungsten carbides and nitrides and ternary systems based on them: the electronic structure, chemical bonding and properties *Russ. Chem. Rev.* **79** 611
[13] Tsaur B Y, Mayer J W and Tu K N 1980 Ion-beam induced metastable Pt_2Si_3 phase. I. Formation, structure and properties *J. Appl. Phys.* **51** 5326
[14] Suetin D V, Shein I R and Ivanovskii A L 2011 Structural, electronic and magnetic properties of tungsten oxycarbides $WC_{1-x}O_x$ and $WO_{3-x}C_x$ from first principles calculations *Phys. Status Solidi* b **248** 2884
[15] Oganov A R and Glass C W 2006 Crystal structure prediction using ab initio evolutionary techniques: principles and applications *J. Chem. Phys.* **124** 244704
[16] Glass C W, Oganov A R and Hansen N 2006 USPEX—evolutionary crystal structure prediction *Comput. Phys. Commun.* **175** 713
[17] Lyakhov A O, Oganov A R and Valle M 2010 How to predict very large and complex crystal structures *Comput. Phys. Commun.* **181** 1623
[18] Blöchl P E 1994 Projector augmented-wave method *Phys. Rev.* B **50** 17953
[19] Kresse G and Joubert D 1999 From ultrasoft pseudopotentials to the projector augmented-wave method *Phys. Rev.* B **59** 1758
[20] Kresse G and Hafner J 1993 *Ab initio* molecular dynamics for liquid metals *Phys. Rev.* B **47** 558
[21] Kresse G and Furthmüller J 1996 Efficient iterative schemes for *ab initio* total-energy calculations using a plane-wave basis set *Phys. Rev.* B **54** 11169
[22] Kresse G and Furthmüller J 1996 Efficiency of ab-initio total energy calculations for metals and semiconductors using a plane-wave basis set *Comput. Mater. Sci.* **6** 15
[23] Perdew J P, Burke K and Ernzerhof M 1996 Generalized gradient approximation made simple *Phys. Rev. Lett.* **77** 3865
[24] Koepernik K and Eschrig H 1999 Full-potential nonorthogonal local-orbital minimum-basis band-structure scheme *Phys. Rev.* B **59** 1743
[25] Palmer D J and Dickens P G 1979 Tungsten dioxide: structure refinement by powder neutron diffraction *Acta Crystallogr.* B **35** 2199
[26] Leciejewicz J 1961 A note on the structure of tungsten carbide *Acta Crystallogr.* **14** 200
[27] Porrati F, Sachser R, Strauss M, Andrusenko I, Gorelik T, Kolb U, Bayarjargal L, Winkler B and Huth M 2010 Artificial granularity in two-dimensional arrays of nanodots fabricated by focused-electron-beam-induced deposition *Nanotechnology* **21** 375302
[28] Momma K and Izumi F 2011 VESTA 3 for three-dimensional visualization of crystal, volumetric and morphology data *J. Appl. Crystallogr.* **44** 1272